Journal of Alloys and Compounds 509 (2011) 5142–5146

Contents lists available at ScienceDirect

Journal of Alloys and Compounds

journal homepage: www.elsevier.com/locate/jallcom

Effect of antimony on vigorous interfacial reaction of Sn–Sb/Te couples

Ching-Hua Lee, Wen-Tai Chen, Chien-Neng Liao*

Department of Materials Science and Engineering, National Tsing-Hua University, 101 Sec. 2 Kuang-Fu Rd., Hsinchu 30013, Taiwan, ROC

ARTICLE INFO

Article history:
Received 19 October 2010
Received in revised form 1 February 2011
Accepted 1 February 2011
Available online 3 March 2011

Keywords:
Thermoelectric
Interfacial reaction
Intermetallic compounds

ABSTRACT

A vigorous reaction between molten Sn–Sb solder and Te substrate leads to a thick SnTe–Sn mixture layer at the soldered junction. The effect of Sb addition in Sn on the kinetics of Sn–Sb/Te interfacial reaction and formation of SnTe–Sn reaction layer is reported. Sb element was found to expedite the growth of SnTe–Sn reaction layer in the Sn–Sb/Te couples dramatically. With increasing Sb content in Sn–Sb solder, the growth rate of SnTe–Sn reaction layer increases while both the size of SnTe grains and the fraction of Sn in SnTe–Sn decrease. The thickness of SnTe–Sn layer follows a parabolic law with reaction time for Sn–Sb/Te couples, unlike the linear dependence with time for Sn/Te couples. An apparent diffusivity of 2×10^{-7} cm^2/s was determined for Sn transport through the SnTe–Sn layer in the Sn–Sb/Te couples reacting at 250 °C.

1. Introduction

Thermoelectric devices can be used to convert thermal energy into electricity directly or pump heat against thermal gradient by supplying electricity [1,2]. Recent thermoelectric research effort is primary focused on development of nanostructured thermoelectrics in order to raise conversion efficiency between thermal and electrical energies [3–5]. In addition to thermoelectrics, the contact properties between metal electrode and thermoelectrics are also known to affect performance and reliability of thermoelectric modules. For high-temperature thermoelectric modules, thermoelectrics are joined to metal electrodes by solid-state reaction or tape casting methods [6,7]. On the other hand, soldering technique is commonly utilized in joining metal electrodes and Bi–Te based compounds, the best-known low-temperature thermoelectrics, for thermoelectric modules operating below 200 °C. Some Sn-based solders such as pure Sn, Sn–Bi, Sn–Pb, Sn–Ag and Sn–Ag–Cu alloys have been employed in assembling thermoelectric modules for different operation requirements. In order to prevent electrical and mechanical degradation of soldered junctions in thermoelectric modules, a 3–5 μm-thick Ni layer is generally coated on both sides of thermoelectrics before soldering onto metal electrodes. However, the Ni layer would be consumed constantly by forming Ni_3Sn_4 compound when the module operates at elevated temperature. Once the Ni layer is consumed completely at some junction locations, Sn will react with bismuth telluride readily by forming SnTe compound that would degrade the mechanical strength of the soldered junctions due to its brittle nature. Therefore, knowledge of interfacial reactions between solder and telluride in thermoelectric modules is of great importance for reliability consideration.

Interfacial reaction layer is known to affect electrical, thermal and mechanical properties of soldered junctions, and hence reliability of thermoelectric modules [8–10]. SnTe has been reported to be the major compound phase in the reaction layer at bismuth telluride/solder junctions [11,12]. With various solder ingredients, the reaction layer may include SnTe as well as other telluride compounds, such as PbTe and CdTe [11]. Chen and Chiu found that the reaction layer formed between molten Sn and Te substrate at 250 °C indeed is a two-phase mixture of SnTe and Sn [13]. The presence of SnTe–Sn reaction layer is speculated to be attributed to the vigorous reaction between Sn and Te because molten Sn can constantly penetrate the loosely bound SnTe compounds to react with Te substrate, leaving a layer of SnTe compound with trapped Sn phase. Moreover, the growth kinetics of the reaction layer in Sn/Te couples can be modulated by some trace elements such as Bi, Ag and Cu in the solder alloys. For example, Bi in molten solder acts as a transport blockade for Sn penetrating through the reaction layer, and the growth rate of the reaction layer decreases with increasing Bi content in Sn [14]. Our previous studies revealed that a small addition of Ag or Cu in Sn solder is sufficient to suppress vigorous Sn/Te reaction by forming a thin barrier layer of Ag–Te or Cu–Te compounds [15,16]. These studies, in common, have shown that trace elements in molten solder tend to inhibit the growth of SnTe–Sn reaction layer. However, an extremely fast reaction was found between molten Sn–Ag–Cu solder and $(Bi,Sb)_2Te_3$ by forming a 13 μm-thick reaction layer within 1–2 s at the soldering temperature [12]. Such a fast growth of reaction layer is rarely seen in typical soldering reactions [17–19]. Because the vigorous Sn–Te reaction was not observed at the soldered junctions of $Bi_2(Se,Te)_3$ thermoelectric elements, the extremely fast growth of reaction layer is likely associated with Sb in $(Bi,Sb)_2Te_3$ thermoelectric elements. In

* Corresponding author. Tel.: +886 35723848; fax: +886 35722366.
E-mail address: cnliao@mx.nthu.edu.tw (C.-N. Liao).

0925-8388/$ – see front matter © 2011 Elsevier B.V. All rights reserved.
doi:10.1016/j.jallcom.2011.02.011

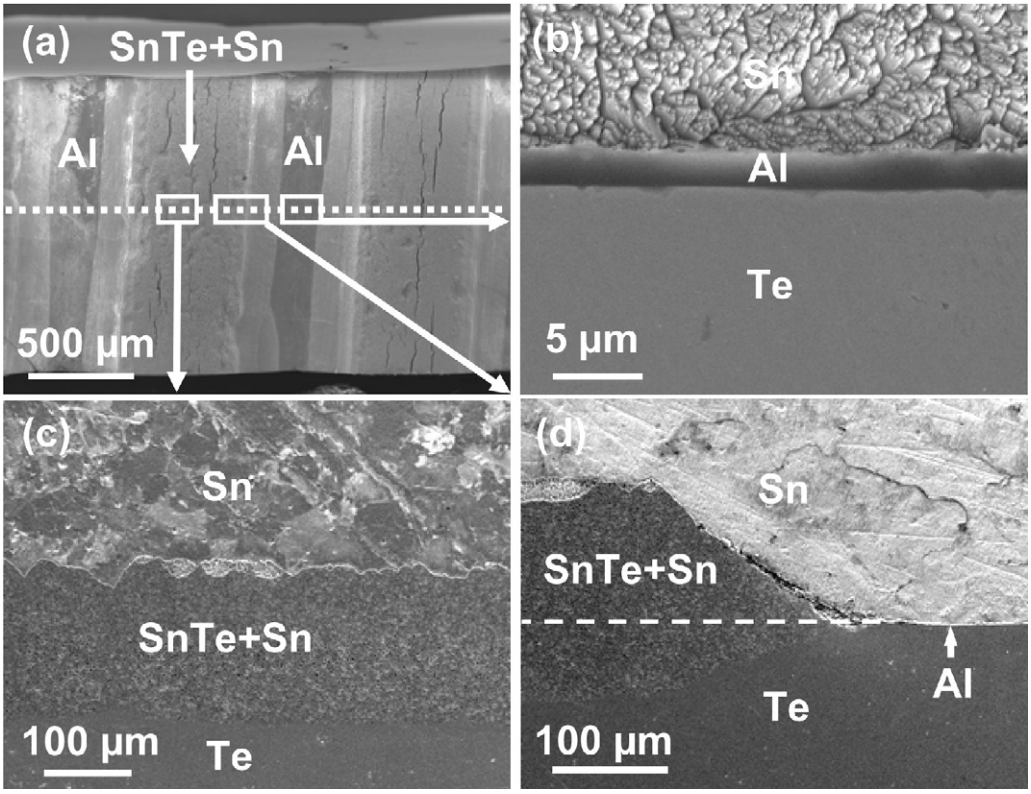

Fig. 1. SEM micrographs of a Sn/Te couple after reacting at 250 °C for 45 min: (a) planar view; (b) cross-sectional view of the Al-passivated region; (c) cross-sectional view of the Al-free region; (d) cross-sectional view of the partially Al-passivated region.

this study, the effect of Sb addition in Sn solder on the vigorous reaction between Sn–Sb solder and Te substrate is reported. The kinetics of Sn–Sb/Te interfacial reaction and formation of SnTe–Sn layer is also investigated.

2. Experimental

Sn–*x*Sb solder alloys of various Sb contents (*x* = 0.1, 0.5, 1, 2, 3 wt.%) were prepared by mixing high-purity Sb powders (99.9 wt.%, ProChem.) and Sn shots (99.99 wt.%, ADMAT) in quartz capsules sealed in vacuum and keeping the capsules in a furnace at 800 °C for 6 days. After being quenched in ice water, the Sn–*x*Sb alloys were chopped into small pieces for subsequent soldering reactions. To prepare rectangular shaped Te substrate, pure Te slugs (99.999 wt.%, ADMAT) were vacuum-sealed in quartz capsules, re-melted at 530 °C, solidified and cut into rectangular plates of 10 mm × 6 mm × 2 mm in size. These rectangular Te plates were carefully polished and then cleaned consecutively with acetone, isopropyl alcohol and de-ionized water in an ultrasonic bath to ensure high-quality soldering surface. Because Al metallization is chemically inert to both tellurium and solder, some Al stripes of 2 μm in thickness were patterned on Te substrate surface to mark the original solder/Te interface for subsequent cross-sectional inspection. The Sn–*x*Sb/Te soldering reactions were performed by putting 2 g of Sn–*x*Sb solder and a Te plate into a sealed quartz tube that were kept at 250 °C for different amount of time ranging from 5 to 45 min. A pure Sn/Te couple was also prepared and examined for comparisons. Fig. 1 shows (a) planar and (b)–(d) cross-sectional images of a Sn/Te couple after reacting at 250 °C for 45 min, which were inspected by scanning electron microscopy (SEM). It is noted that a thick reaction layer (SnTe + Sn) was observed in the Al-free region (Fig. 1(c)), while no reaction layer in the Al-passivated region (Fig. 1(b)). In addition, a beak-shaped compound layer was found near the edge of the Al strip due to lateral penetration and reaction of Sn with Te underneath the Al strip (Fig. 1(d)). All the samples were ground, polished, and etched slightly with CH_3OH (93 vol.%) – HCl (2 vol.%) – HNO_3 (5 vol.%) solution to unveil the interfacial structure of the soldered junctions. Some of the samples were intentionally etched away unreacted solder by dilute HNO_3 (13 vol.%) to reveal the morphology of the SnTe compounds. The morphology and composition of the reaction layer were examined by SEM (JEOL JSM-6500F, Tokyo, Japan) and electron probe microanalyzer (EPMA, JEOL JXA-8800M, Tokyo, Japan). An X-ray diffraction (XRD) analysis was conducted to identify the interfacial compounds using an X-ray diffractometer (SHIMADZU-6000, Kyoto, Japan) with Cu Kα line source. An image analyzer (Optimas, USA) was utilized to measure the thickness of reaction layer and the size of SnTe grains.

3. Results and discussion

Fig. 2 shows cross-sectional SEM micrographs of Sn/Te and Sn–1Sb/Te couples after reacting at 250 °C for 15 min. Fig. 2(a) and (b) shows the Al-free region, while Fig. 2(c) and (d) the partially Al-passivated region of the Sn/Te and Sn–1Sb/Te couples. The sample surface has been slightly etched to differentiate the SnTe–Sn reaction layer from solder and Te substrate because the SnTe–Sn layer has uniformly distributed pits on surface due to preferential Sn etching. The Sn–1Sb/Te couple has similar but much smaller pits in the SnTe–Sn layer, which can be seen in the magnified image shown in the inset of Fig. 2(b). The SnTe–Sn thicknesses were found to be 60 and 370 μm for the Sn/Te and Sn–1Sb/Te couples, respectively. Such a high growth rate is rarely seen in typical soldering reactions. For examples, Sn/Ni and Sn/Cu couples only have 4–5 μm-thick Ni_3Sn_4 and Cu_6Sn_5 interfacial compounds, respectively, after reacting at 250 °C for 10 min [17,19]. The high growth rate of SnTe–Sn reaction layer is believed to be associated with high diffusivity of Sn through the SnTe–Sn reaction layer and SbSn-enhanced heterogeneous nucleation at the interface, which will be discussed subsequently. Because the reaction layer is a mixture of SnTe and Sn, we can estimate the fraction of Sn in SnTe–Sn by evaluating the amount of Te consumption and SnTe formation. In the vicinity of Al-passivated region the beak-shaped compound helps identify the original solder/Te interface and estimate the Te consumption, as shown in Fig. 2(c) and (d). Theoretically, the thickness of SnTe, t_{SnTe}, formed during soldering reaction can be calculated from the amount of Te consumed, t_{Te}, as follows.

$$t_{SnTe} = t_{Te}\left(\frac{M_{SnTe}}{M_{Te}}\frac{\rho_{Te}}{\rho_{SnTe}}\right) \quad (1)$$

where M and ρ stand for molecular (atomic) weight and density of SnTe (Te), respectively. Assuming the Sn phase is uniformly distributed in the reaction layer of thickness $t_{SnTe-Sn}$, the fraction of

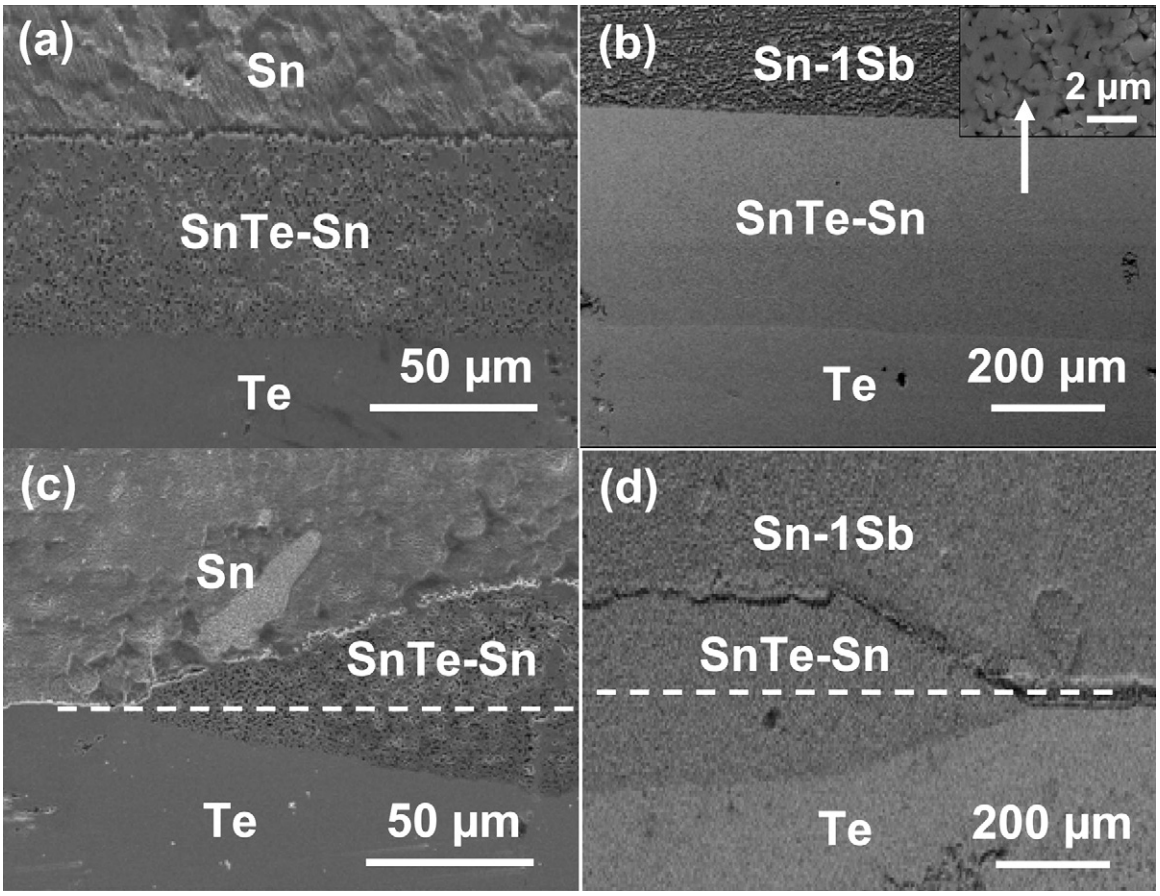

Fig. 2. Cross-sectional SEM micrographs of Sn/Te and Sn–1Sb/Te couples after reacting at 250 °C for 15 min: (a) and (b) Al-free region; (c) and (d) partially Al-passivated region.

Sn in SnTe–Sn, f_{Sn}, is thus given by

$$f_{Sn} = 1 - \left(\frac{t_{SnTe}}{t_{SnTe-Sn}}\right) \quad (2)$$

Fig. 3 shows the thickness of SnTe–Sn layer and the fraction of Sn in SnTe–Sn against reaction time for the Sn/Te and Sn–1Sb/Te couples reacting at 250 °C. Interestingly, the SnTe–Sn thickness of the Sn–1Sb/Te couple increases non-linearly with reaction time, but

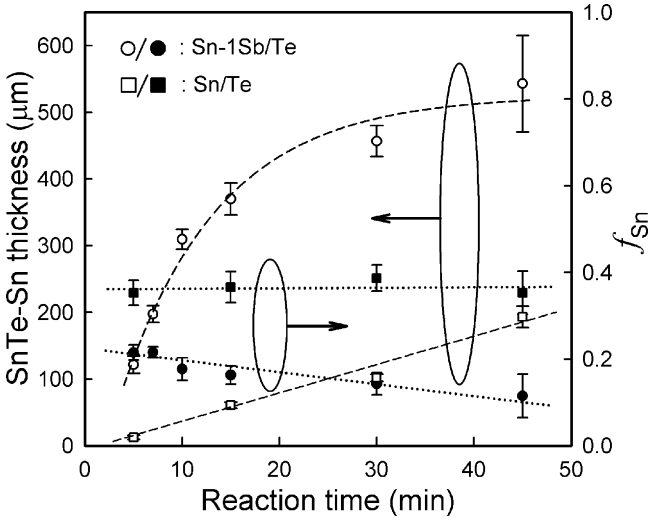

Fig. 3. Plots of SnTe–Sn layer thickness and Sn fraction in SnTe–Sn layer of the Sn/Te and Sn–1Sb/Te couples as a function of reaction time at 250 °C.

that of the Sn/Te couple shows a linear dependence with reaction time. Besides, the fraction of Sn in SnTe–Sn of the Sn–1Sb/Te couple decreases from 0.22 to 0.12, while that of the Sn/Te couple remains unchanged around 0.35 with increasing reaction time. By following a similar analysis of thermally grown SiO_2 on Si substrate [20], the thickness of SnTe–Sn layer formed during soldering reaction is given by

$$t_{SnTe-Sn} = \frac{D}{k}\left[\left(1 + \frac{2k^2N}{nD}t\right)^{1/2} - 1\right] \quad (3)$$

where D, k, N and n are diffusivity of Sn in the SnTe–Sn layer, rate constant of Sn/Te reaction, Sn concentration in solder and Sn concentration in the SnTe–Sn, respectively. If the reaction time t is long enough, $t_{SnTe-Sn}$ is further reduced to

$$t_{SnTe-Sn} = \left(\frac{2ND}{n}\right)^{1/2} t^{1/2} \quad (4)$$

Fig. 4 shows the thickness of SnTe–Sn measured with respect to the square root of reaction time for the Sn–1Sb/Te couple. The apparent diffusivity of Sn in the SnTe–Sn layer is determined to be 2×10^{-7} cm^2/s from the slope of the plot in the latter stage of reaction according to Eq. (4). It is noted that the Sn diffusivity in SnTe is $\sim 10^{-13}$ cm^2/s at 475 °C [21], while the Sn self-diffusivity in liquid Sn is 2.5×10^{-5} cm^2/s at 250 °C [22]. The results imply that Sn must diffuse mainly through liquid Sn rather than SnTe in the SnTe–Sn mixture layer.

Now, the question is how Sb element affects the reaction between Sn and Te as well as the growth kinetics of SnTe–Sn reaction layer in Sn–Sb/Te couples. Fig. 5 shows the thickness and

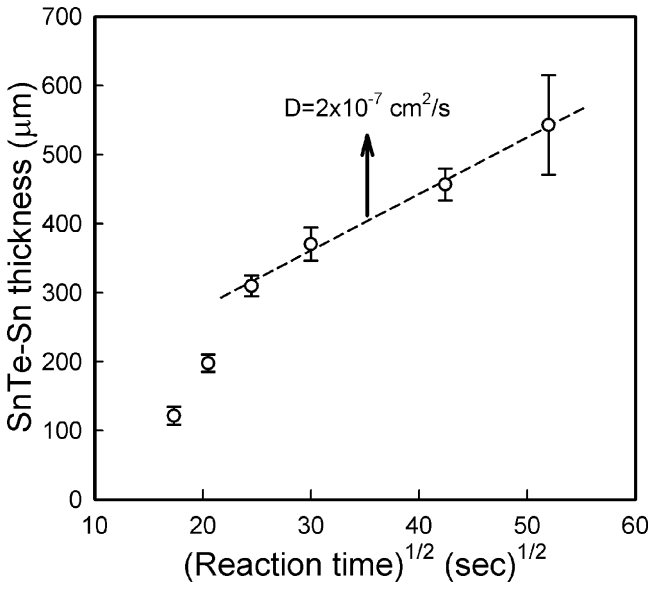

Fig. 4. A plot of SnTe–Sn layer thickness versus square root of reaction time for the Sn–1Sb/Te couple reacting at 250 °C.

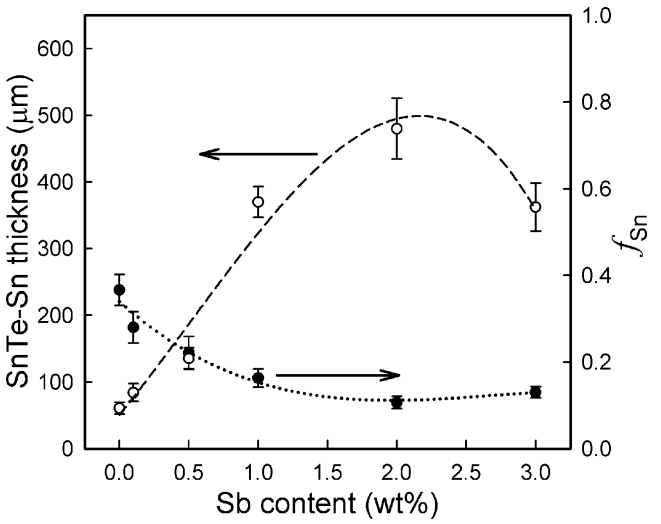

Fig. 5. Plots of SnTe–Sn layer thickness and Sn fraction in SnTe–Sn layer with respect to Sb content in the Sn–*x*Sb/Te couples (*x* = 0–3 wt.%) reacting at 250 °C for 15 min.

the Sn fraction of the SnTe–Sn layer with respect to Sb content in Sn–*x*Sb/Te couples (*x* = 0–3 wt.%) reacting at 250 °C for 15 min. With increasing Sb content, $t_{SnTe-Sn}$ increases up to a maximum at 2 wt.% Sb and decreases at 3 wt.% Sb, while f_{Sn} decreases monotonically from 0.35 to 0.12. It is worthy of mentioning that the linear dependence of $t_{SnTe-Sn}$ on reaction time for Sn/Te couples, shown in Fig. 3, follows a reaction-controlled kinetics [13]. However, the parabolic-like growth of SnTe–Sn layer with reacting time suggests that the diffusion of Sn through the SnTe–Sn layer may become the rate-limiting step for Sn–1Sb/Te couples. The decreasing f_{Sn} implies the reduction of Sn diffusion channel volume in the SnTe–Sn layer, which would limit the supply of Sn reacting with Te substrate. Fig. 6 shows the top-view SEM images of the Sn–*x*Sb/Te couples (*x* = 0, 1, 2 and 3 wt.%) after reacting at 250 °C for 15 min

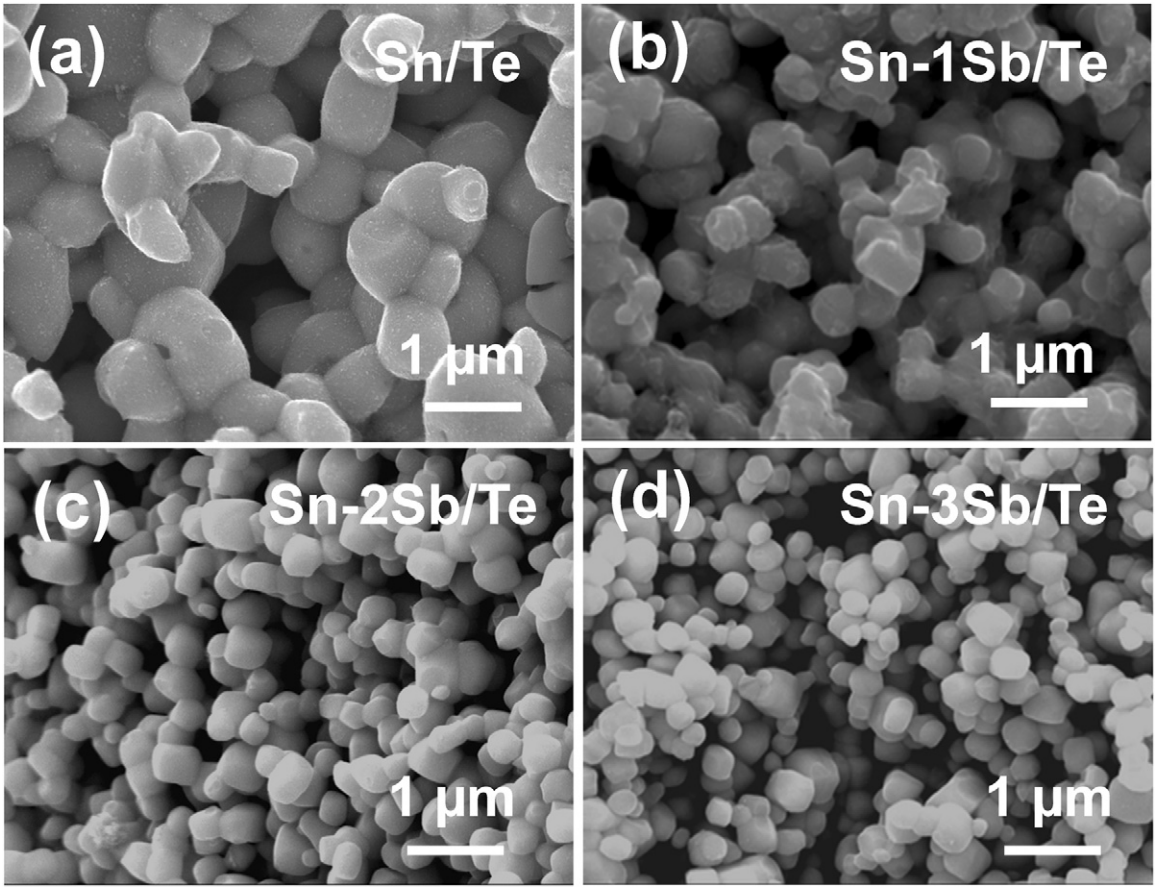

Fig. 6. The top-view SEM images of the Sn–*x*Sb/Te couples (*x* = 0, 1, 2 and 3 wt.%) after reacting at 250 °C for 15 min and etching away unreacted Sn.

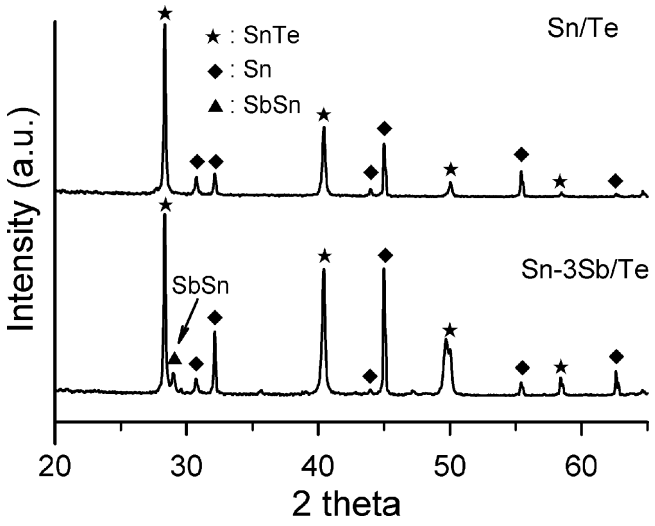

Fig. 7. XRD results of the Sn/Te and Sn–3Sb/Te couples after reacting at 250 °C for 15 min.

and etching away unreacted Sn to reveal the SnTe morphology. Apparently, the higher the Sb content in Sn solder, the more and the smaller the SnTe grains in the reaction layer. The observation is consistent with the reducing f_{Sn} in the SnTe–Sn layer. According to the Sb–Sn–Te ternary phase diagram, SbSn would precipitate along with SnTe at very small Sb content in the temperature between 220 °C and 300 °C [23]. The presence of SbSn is expected to enhance the nucleation of SnTe grains in the SnTe–Sn layer. Indeed, the phenomenon of SbSn-enhanced heterogeneous nucleation of Cu_6Sn_5 has also been reported for Sn–Ag–Cu–Sb solder when reacting with Cu substrate [24]. Thus, a vigorous growth of abundant SnTe grains at the Sn–Sb/Te interface leads to small f_{Sn} and reduced effective Sn diffusivity through the SnTe–Sn layer. For a Sn–Sb/Te couple with higher Sb content, the transition of reaction to diffusion controlled kinetics would occur at the earlier reaction stage due to the SbSn-enhanced SnTe nucleation rates. Therefore, with the same reaction time at 250 °C the SnTe–Sn layer in the Sn–3Sb/Te couple is thinner than that in the Sn–2Sb/Te couple, as shown in Fig. 5. To confirm the presence of SbSn phase, an XRD analysis was performed on the Sn/Te and Sn–3Sb/Te couples after reacting at 250 °C for 15 min, which were carefully polished to remove the solder cap to expose the SnTe–Sn reaction layer. The results indicate that SbSn phase indeed exists in the Sn–3Sb/Te couple but not in the Sn/Te couple, as shown in Fig. 7. In summary, the presence of Sb in Sn solder can lead to the formation of SbSn phase that serves as nucleation agents for SnTe nuclei. Thus, there are many refined SnTe grains in the SnTe–Sn reaction layer of the Sn–Sb/Te couples with high Sb content. However, a large amount of SnTe grains formed simultaneously would decrease the effective Sn diffusivity through SnTe–Sn, and slow down the growth of SnTe–Sn layer.

4. Conclusions

The effect of Sb addition in Sn solder on the kinetics of interfacial reaction and growth of SnTe–Sn reaction layer was investigated. With increasing Sb content in Sn solder, the growth rate of SnTe–Sn layer increases significantly due to SbSn enhanced SnTe nucleation rate. The SnTe–Sn layer in the Sn–Sb/Te couples of high Sb content contains many small SnTe grains and owns small fraction of Sn phase. The thick SnTe–Sn reaction layer in the Sn–Sb couples changes the rate-limiting step from Sn–Te reaction to Sn diffusion through the reaction layer, and thus the SnTe–Sn thickness increases proportionally with square root of reaction time. The reduced fraction of Sn in the SnTe–Sn layer causes the reaction-to-diffusion transition to occur at early stage for the Sn–Sb/Te couples of high Sb content.

Acknowledgement

The work is supported by National Science Council of the Republic of China through grant no. NSC 98-3114-E-007-008.

References

[1] F.J. DiSalvo, Science 285 (1999) 703–706.
[2] L.E. Bell, Science 321 (2008) 1457–1461.
[3] B. Poudel, Q. Hao, Y. Ma, Y. Lan, A. Minnich, B. Yu, X. Yan, D. Wang, A. Muto, D. Vashaee, X. Chen, J. Liu, M.S. Dresselhaus, G. Chen, Z. Ren, Science 320 (2008) 634–638.
[4] P.X. Lu, F. Wu, H.L. Han, Q. Wang, Z.G. Shen, X. Hu, J. Alloys Compd. 505 (2010) 255–258.
[5] A. Popescu, L.M. Woods, Appl. Phys. Lett. 97 (2010) 052102.
[6] D. Zhao, X. Li, L. He, W. Jiang, L. Chen, J. Alloys Compd. 477 (2009) 425–431.
[7] K. Park, J.W. Choi, C.W. Lee, J. Alloys Compd. 486 (2009) 785–789.
[8] J.H. Kiely, D.V. Morgan, D.M. Rowe, Semicond. Sci. Technol. 9 (1994) 1722–1728.
[9] T.M. Ritzer, P.G. Lau, A.D. Bogard, Proc. 16th Int. Conf. on Thermoelectrics, Dresden, Germany, August 26–29, 1997, pp. 619–623.
[10] K.A. Moores, Y.K. Joshi, G. Miller, Proc. 18th Int. Conf. on Thermoelectrics, Baltimore, MD, USA, August 29–September 2, 1999, pp. 31–34.
[11] T.D. Alieva, B.S. Barkhalov, D.S. Abdinov, Inorg. Mater. 31 (1995) 178–182.
[12] C.N. Liao, C.H. Lee, W.J. Chen, Electrochem. Solid State Lett. 10 (2007) P23–P25.
[13] S.W. Chen, C.N. Chiu, Scripta Mater. 56 (2007) 97–99.
[14] C.N. Chiu, C.H. Wang, S.W. Chen, J. Electron. Mater. 37 (2008) 40–44.
[15] C.N. Liao, Y.C. Huang, J. Mater. Res. 25 (2010) 391–395.
[16] C.N. Liao, C.H. Lee, J. Mater. Res. 23 (2008) 3303–3308.
[17] S.J. Wang, C.Y. Liu, J. Electron. Mater. 32 (2003) 1303–1309.
[18] S.W. Chen, A.R. Zi, P.Y. Chen, H.J. Wu, Y.K. Chen, C.H. Wang, Mater. Chem. Phys. 111 (2008) 17–19.
[19] C.M. Liu, C.E. Ho, W.T. Chen, C.R. Kao, J. Electron. Mater. 30 (2001) 1152–1156.
[20] S.K. Ghandhi, VLSI Fabrication Principles: Silicon and Gallium Arsenide, 2nd ed., John Wiley & Sons, New York, 1994, pp. 458–461.
[21] H. Scherrer, G. Pineau, S. Scherrer, Phys. Lett. A 75 (1979) 118–120.
[22] C.H. Ma, R.A. Swalin, J. Chem. Phys. 36 (1962) 3014–3018.
[23] A. Stegherr, in: P. Villars, A. Prince, H. Okamoto (Eds.), Handbook of Ternary Alloy Phase Diagrams, ASM International, Materials Park, OH, 1994, pp. 13492–13495.
[24] B.L. Chen, G.Y. Li, Thin Solid Films 462 (2004) 395–401.